

Topological Properties of Single-Particle States Decaying into a Continuum due to Interaction

B. Hawashin,^{1,2,*} J. Sirker,^{2,†} and G. S. Uhrig^{1,‡}

¹*Condensed Matter Theory, Department of Physics,
TU Dortmund University, Otto-Hahn-Straße 4, 44221 Dortmund, Germany*

²*Department of Physics and Astronomy and Manitoba Quantum Institute,
University of Manitoba, Winnipeg R3T 2N2, Canada*

(Dated: July 30, 2024)

We investigate how topological Chern numbers can be defined when single-particle states hybridize with continua. We do so exemplarily in a bosonic Haldane model at zero temperature with an additional on-site decay of one boson into two and the conjugate fusion of two bosons into one. Restricting the Hilbert space to two bosons at maximum, the exact self-energy is accessible. We use the bilinear Hamiltonian H_0 corrected by the self-energy Σ to compute Chern numbers by two different approaches. The results are gauged against a full many-body calculation in the Hilbert space where possible. We establish numerically and analytically that the effective Hamiltonian $H_{\text{eff}} = H_0(\vec{k}) + \Sigma(\omega, \vec{k})$ reproduces the correct many-body topology if the considered band does not overlap with the continuum. In case of overlaps, one can extend the definition of the Chern number to the non-Hermitian H_{eff} and there is evidence that the Chern number changes at exceptional points. But the bulk-boundary correspondence appears to be no longer valid and edge modes delocalize.

Introduction The first striking topological effect discovered in condensed matter physics is the integer quantum Hall effect [1]. Here, the number of contributing edge modes defines the Hall conductivity [2, 3] to an incredible precision revolutionizing metrology [4]. No nonlinearities occur [5, 6]. Also, fractional charges are possible enabling the fractional quantum Hall effect [7]. Both topological effects gained their discoverers Nobel Prizes [8, 9] and topology in condensed matter has continued to gain great interest in the last decades [10]. The possible types of topological order have been classified for Gaussian fermionic systems, both in the case of non-spatial and spatial symmetries [11–16]. A non-trivial topological ground state of a fermionic insulator cannot be connected adiabatically to the atomic limit without closing the gap or, if present, breaking the symmetry protecting the topological order. These topological states thus have non-trivial entanglement and typically also robust edge states [17–21]. For quantum Hall systems, in particular, topologically non-trivial ground states were proposed even for models without external magnetic field [22] and realized in experiment [23–26]. Numerous technological applications are expected not only in fermionic systems [27–30] but also in insulating quantum magnets, see e.g. Ref. [31].

A crucial aspect of quantum Hall systems breaking time reversal symmetry is the occurrence of robust, chiral edge modes which generically allow for motion only in one direction. These systems promise a high degree of tunability [32, 33]. The number of these chiral edge modes is linked to the Chern number of a dispersive band, i.e., a topological invariant given by the Berry phase of a quantum state tracked around the Brillouin zone (BZ).

This is commonly referred to as the bulk-boundary correspondence [34, 35]. However, already for non-interacting systems, this correspondence must be used with caution because it only holds if the dispersive band is protected by *indirect* energy gaps [36, 37]. Otherwise, the potential boundary mode is not localized, but extends into the continuum. Such a breakdown of the bulk-boundary correspondence can also occur in manifestly non-Hermitian systems [38–42].

Thus, the hybridization of modes with continua can destroy the desired topological properties. Clearly, if a single-particle excitation is no longer defined in the whole BZ, its Berry connection [43] cannot be defined in the standard way. Such a hybridization of single-particle states with continua is generic in interacting systems. Hence, a generalization of topological invariants is required. For ground states of fermionic topological insulators, topological invariants such as the Chern number can be expressed in terms of Green’s functions at zero frequency [44–46]. Clearly, this allows for a straightforward extension to systems with interactions although zeroes in the Green’s function need to be considered carefully. The appearance of edge modes at zero energy at the boundary between two topologically distinct phases is then the generic scenario, supporting the bulk-boundary correspondence. Similarly, a classification of symmetry-protected topological phases in interacting bosonic systems based on group cohomology theory exists [47].

Here, we do not focus on the ground state and its topological properties but rather on the bands of elementary, single-particle excitations. Without interactions, the Berry curvature is unambiguously defined. Including interactions, two situations need to be distinguished: (i)

If the single-particle states are adiabatically connected to the ones in the absence of interactions, i.e., the hybridization renormalizes the single-particle states, then the Chern number can be defined in a mathematically rigorous way and the bulk-boundary correspondence holds if the edge mode is protected by an energy gap. (ii) If the single-particle states hybridize strongly with the continua, so that they merge with them, a Chern number can be defined for the non-Hermitian effective Hamiltonian, but not for the full Hamiltonian. The bulk-boundary correspondence appears not to be valid in this case.

We define a bosonic model reduced to the essentials which allows for various approaches to treat it. Our study provides evidence that the self-consistent solution of the effective single-particle problem defined by the non-interacting Hamiltonian plus the proper self-energy is the appropriate generalization to calculate Chern numbers in the interacting case. This approach provides a connection between many-particle Hermitian models and single-particle non-Hermitian models. We emphasize, however, that usually non-Hermiticity is invoked on the basis of gains and losses. Here, in contrast, we investigate a Hermitian many-body problem which can be reduced to an effective single-particle problem if the complex self-energy with its full frequency dependence is known. This effective problem can be non-Hermitian, but its non-Hermiticity depends on frequency.

Model We consider interacting bosons on a honeycomb lattice with sublattices A and B sites described by

$$H = H_0 + H_{\text{int}} \quad (1a)$$

$$H_0 = t_1 \sum_{\langle i,j \rangle} \left(b_i^\dagger b_j + \text{h.c.} \right) + t_2 \sum_{\langle\langle i,j \rangle\rangle} \left(e^{i\nu_{ij}} \phi b_i^\dagger b_j + \text{h.c.} \right) + M \sum_i \varepsilon_i b_i^\dagger b_i + E_0 \sum_i b_i^\dagger b_i \quad (1b)$$

$$H_{\text{int}} = g \sum_i \left(b_i^\dagger b_i^\dagger b_i + \text{h.c.} \right), \quad (1c)$$

where b_i and b_i^\dagger are bosonic annihilation and creation operators, respectively. The prefactors $t_1, t_2, g, E_0 \in \mathbb{R}^+$ and $M \in \mathbb{R}$ are energies, $\nu_{ij} = +1$ if hopping from i to j is clockwise in a hexagon and $\nu_{ij} = -1$ otherwise. The local sign is $\varepsilon_i = 1$ if $i \in A$ and $\varepsilon_i = -1$ if $i \in B$. The sums over $\langle i, j \rangle$ and $\langle\langle i, j \rangle\rangle$ run over nearest neighbors and next-nearest neighbors, respectively. This bilinear part is analogous to the fermionic Haldane model which displays well-established topological properties with finite Chern numbers [22]. The on-site energy E_0 serves two purposes: first, E_0 needs to be sufficiently large so that the bosonic excitation energies are positive. Then, the ground state is the topologically trivial bosonic vacuum. Our focus is on the topological properties of the excited bands. Second, tuning E_0 and g allows to control the strength of the hybridization between one-boson and two-boson states.

The cubic interaction H_{int} describes the decay of one boson into two bosons on the same site with coupling constant g or the inverse process, i.e., the fusion of two bosons into one. Terms of this kind occur generically in quantum magnets for spin waves in case of non-collinear order [48–50] as well as for triplons in valence bond solids [50–53]. We stress that one should first perform a Bogoliubov transformation to diagonalize the bilinear part including terms of two annihilation or creation operators. Otherwise, it is unavoidable to generalize the operator scalar product to a symplectic or paraunitary one, see for instance Refs. [36, 54, 55]. The diagonalized Hamiltonian is similar to (1) except that the hopping terms and the interaction terms have a certain spatial range. In this sense, H is an idealization adopted here not to be distracted by a plethora of parameters. We consider the cubic interaction because the continuum to which the single-particle states are coupled is then governed by only one free momentum while the relevant continuum for the quartic interaction requires two free momenta. Thus, the treatment of cubic terms is considerably easier than the one of quartic terms. The possibility of having cubic interactions is also a reason to consider a bosonic instead of a fermionic model where cubic terms do not occur in standard systems.

In order to deal with an exactly solvable limit, we restrict the Hilbert space to $\mathcal{H} = \mathcal{H}(0) \oplus \mathcal{H}(1) \oplus \mathcal{H}(2)$, where $\mathcal{H}(n)$ is the Hilbert space of exactly n bosons. Hence, the restriction allows for two bosons at maximum. Then, we can exactly determine the self-energy at zero temperature, see the Suppl. Mat. [56]. The efficient evaluation on meshes in the BZ of moderate sizes is carried out by means of a generalized continued fraction expansion derived in the Suppl. Mat. [56]. Alternatively, we can consider the self-energy as the leading contribution in perturbation theory of quadratic order in g . In this view, the Hilbert space does not need to be restricted.

Chern numbers For non-interacting systems, the Chern number of the n -th band is defined as $C = \frac{1}{2\pi} \int_{\text{BZ}} F_{12} d^2k$, where $F_{12} = \partial_1 A_2 - \partial_2 A_1$ denotes the Berry curvature and $A_i(\vec{k}) = \langle u_n(\vec{k}) | \partial_i | u_n(\vec{k}) \rangle$ is the Berry connection. The states $|u_n(\vec{k})\rangle$ are the single-particle states at wave vector \vec{k} . In order to calculate these states, the coefficient matrix $H_0(\vec{k})$ of the bilinear Hamiltonian at this wave vector is sufficient. For the model under study, this amounts to the solution of a 2×2 problem at each given point of a mesh in the BZ. In our calculations, we use meshes ranging from 20×20 to 30×30 . These sizes are sufficient to compute the Chern numbers [57].

We proceed in three distinct ways:

a) Topological approach We use the eigenstates of

$$H_{\text{top}}(\vec{k}) = H_0(\vec{k}) + \Sigma(\omega = 0, \vec{k}) \quad (2a)$$

fulfilling

$$H_{\text{top}}(\vec{k})|u_n(\vec{k})\rangle = E_n(\vec{k})|u_n(\vec{k})\rangle. \quad (2b)$$

Obviously, this is still a 2×2 problem. At zero frequency, the self-energy is Hermitian so that no issues from non-Hermiticity arise; $E_n(\vec{k})$ is real. Wang et al. showed that for fermionic models at $T = 0$ the sum $\sum_{\alpha \text{ occ.}} C_\alpha$ of the Chern numbers C_α obtained from $H_{\text{top}}(\vec{k})$ for the occupied bands provides the Chern number of the ground state which defines the Hall conductivity [45, 58].

b) Effective approach We use the eigenstates of

$$H_{\text{eff}}(\omega, \vec{k}) = H_0(\vec{k}) + \Sigma(\omega, \vec{k}) \quad (3a)$$

fulfilling the self-consistent eigenvalue equation

$$H_{\text{eff}}(E, \vec{k})|u(E, \vec{k})\rangle = E(\vec{k})|u(E, \vec{k})\rangle. \quad (3b)$$

This is still a 2×2 problem, but with the calculation of the self-consistent $E(\vec{k})$ as additional challenge. For non-Hermitian diagonalizations, the right and left eigenstates differ, but they define fiber bundles over the manifold given by the torus of the BZ, allowing for the definition of quantized Chern numbers and it has been shown that they yield the same Chern numbers [38]. In Ref. [59], the suitability of the effective Hamiltonian $H_{\text{eff}}(\omega, \vec{k})$ was critically discussed because it did not provide the correct Chern number of fermionic ground states. Since, however, our focus is a different one it is worthwhile considering $H_{\text{eff}}(E, \vec{k})$.

c) Two-body approach We use the eigenstates at a given total wave vector \vec{k} in the total Hilbert space \mathcal{H}

$$H(\vec{k})|u_n(\vec{k})\rangle = E_n(\vec{k})|u_n(\vec{k})\rangle. \quad (4)$$

This is a standard Hermitian diagonalization problem, but in a large Hilbert space of which the dimension at fixed wave vector \vec{k} is given by the number of sites in the model. Numerically, we deal with sizes of 100 to 1000 sites. The calculation of Berry connections does not pose a conceptual difficulty in the total Hilbert space as long as one can uniquely identify the relevant eigenstates. This is the crucial obstacle in the case of bands overlapping with the continuum.

Phase transition at gap closure In a two-band system, the Chern number of a band does not change if it is only adiabatically modified while staying separated from the other band by a finite gap. Thus, a phase transition between regions of different Chern numbers must be accompanied by the vanishing of the direct energy gap between the two bands, i.e., at some \vec{k}

$$\Delta E(\vec{k}) = |E_1(\vec{k}) - E_2(\vec{k})| = 0. \quad (5)$$

In the Haldane model, the gap closes for the chosen parameters $t_1 = t_2 = 1$, $\phi = \pi/2$ at the K point if $M = 3\sqrt{3}$. We vary M keeping the other parameters fixed and determine M_C where the gap closes. Then, we determine the Chern number in the regions $M < M_C$ and $M > M_C$.

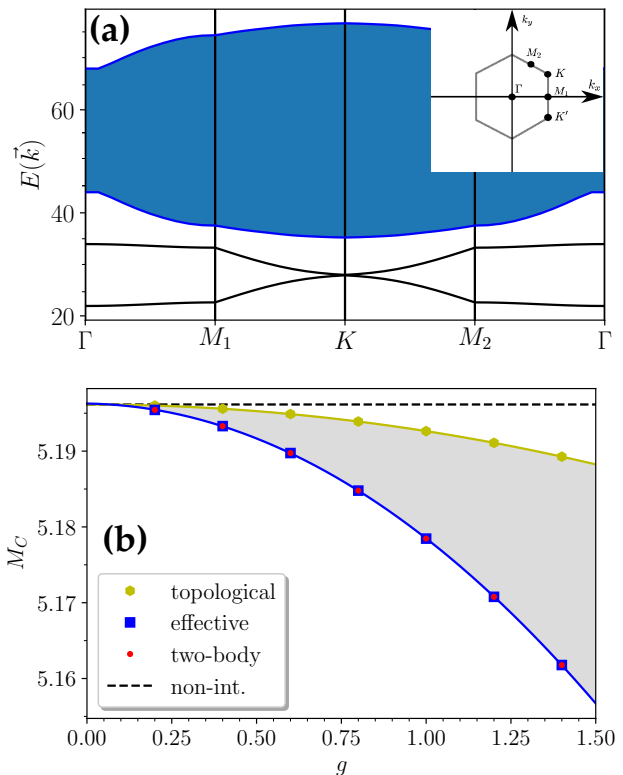


FIG. 1. (a) Two-boson continuum (colored) and renormalized single-boson bands for $E_0 = 28$, $M = 5.2$, and $g = 1.4$. (b) Critical values of M_C where the gap between the single-particle bands closes in the three approaches. Lines are quadratic fits.

Edge states To assess the implications of non-trivial Chern numbers in the interacting case and hence the validity of the bulk-boundary correspondence, we calculate the inverse participation ratio (IPR) [60, 61] on a honeycomb ribbon periodic in x direction with length N_x and finite width N_y in y direction with open boundary conditions, for details see Suppl. Mat. [56]. If the n -th eigenstate is localized, the IPR stays finite $\lim_{N_y \rightarrow \infty} I_n = \text{const}$ while it vanishes $\lim_{N_y \rightarrow \infty} I_n \sim 1/N_y^\alpha \rightarrow 0$ with $\alpha > 0$ for a delocalized state [36] allowing us to determine whether or not a state is localized. Further evidence for (de) localization is obtained from the local density of states (LDOS), also provided in the Suppl. Mat. [56].

Case I: No overlap with the lower band For large $E_0 = 28$ the bands do not overlap with the two-boson continuum, see Fig. 1(a). Panel (b) shows the dependence of M_C on the coupling g . The effect is small because the system is in the perturbative regime where we estimate the self-energy to be $|\Sigma_{ij}| \approx \frac{g^2}{E_0} = 0.07$ for $g = 1.4$ and $E_0 = 28$. Within numerical accuracy, we find that the gap closure occurs at the K point in the BZ in all three approaches. We find $\Sigma(\omega, \vec{k})^\dagger = \Sigma(\omega, \vec{k})$

if $\omega < E_{\min}^{(2)}(\vec{k}) = \min_{\alpha, \beta, \vec{q}} (E_{\alpha}(\vec{k} + \vec{q}) + E_{\beta}(-\vec{q}))$. Thus, we expect and observe only a (weak) renormalization of the non-interacting bands and an infinite lifetime of the excitations.

Due to the absence of overlap between the one-boson bands and the continuum, the Chern numbers are well-defined in all three approaches. We find that $C_{\text{top}} = C_{\text{eff}} = C_{2\text{body}} = 1$ below the grey shaded area in Fig. 1(b), while $C_{\text{top}} = C_{\text{eff}} = C_{2\text{body}} = 0$ above. However, the approaches differ within the shaded area where $C_{\text{top}} = 1$ but $C_{\text{eff}} = C_{2\text{body}} = 0$. The many-body calculation considers the complete quantum state and thus the correct transition amplitudes enter the Berry connection. Hence, we conclude from the agreement of the effective approach with the two-body approach that the effective approach is able to assess the Berry curvature and thus the Chern numbers of the many-body problem *without* conducting an extensive calculation in the complete Hilbert space. The deviating topological approach, while being justified for the ground state of fermionic models with filled bands, is not appropriate for determining the Berry curvature of excitations above the ground state.

The finding, that the effective Hamiltonian including the self-consistency yields exactly the same Berry phases and thus Chern numbers as considering the full Hilbert space, is analytically shown by the following argument. If the total Hilbert space \mathcal{H} can be split into the direct sum of a single-particle part $\mathcal{H}(1)$ and the rest $\mathcal{H}_{\text{rest}}$ so that $\mathcal{H} = \mathcal{H}(1) \oplus \mathcal{H}_{\text{rest}}$ then a generic eigenvector v consists of $v = v_1 + v_{\text{rest}}$. In the Supplement we show that v_1 can be found by solving the self-consistency (3b). Transporting v parallelly around a contour γ yields v' and $\langle v|v' \rangle = \exp(i\varphi)$ implies $v' = \exp(i\varphi)v$ and the Berry phase φ . Thus, in $\mathcal{H}(1)$ the relation $v'_1 = \exp(i\varphi)v_1$ holds so that the Berry phase determined in the subspace $\mathcal{H}(1)$ is identical to the one in the total Hilbert space, see also Suppl. Mat. [56].

In addition, we checked the bulk-boundary correspondence by inspecting the IPR. In case (i) we find clear numerical evidence that localized edge modes exist where the Chern number is different from zero; this is also confirmed by the LDOS, see Suppl. Mat. [56].

We find the same qualitative behavior if the upper band overlaps with the continuum, but not the lower band. Then the Chern number of the lower band is still unambiguously defined and the bulk-boundary correspondence holds.

Case II: Overlap with both bands If both bands overlap with the continuum as shown in Fig. 2 for $E_0 = 16$ and $M = 5.2$, it is not a priori clear if topological properties survive. The topological approach still works as before and yields the upper curve M_C in Fig. 2(b).

But in the two other approaches we encounter major differences to the previous case. In the effective approach, the self-energy becomes non-Hermitian, but the effective Hamiltonian still defines two bands. Their eigenvalues are sufficiently separated in the complex plane so that the eigenvectors are defined unambiguously, except where the gap closes (5), yielding the lower curve in Fig. 2(b). We found numerical evidence that at gap closure, i.e., for $E_1(\vec{k}) = E_2(\vec{k})$, the Chern number changes and that this point is an exceptional point where both eigenvectors point in the same direction, see Suppl. Mat. [56]. Calculating the Chern numbers, we find that $C_{\text{top}} = C_{\text{eff}} = 1$ below the grey shaded area in Fig. 2(b), $C_{\text{top}} = 1$ and $C_{\text{eff}} = 0$ within the shaded area, and $C_{\text{top}} = C_{\text{eff}} = 0$ above.

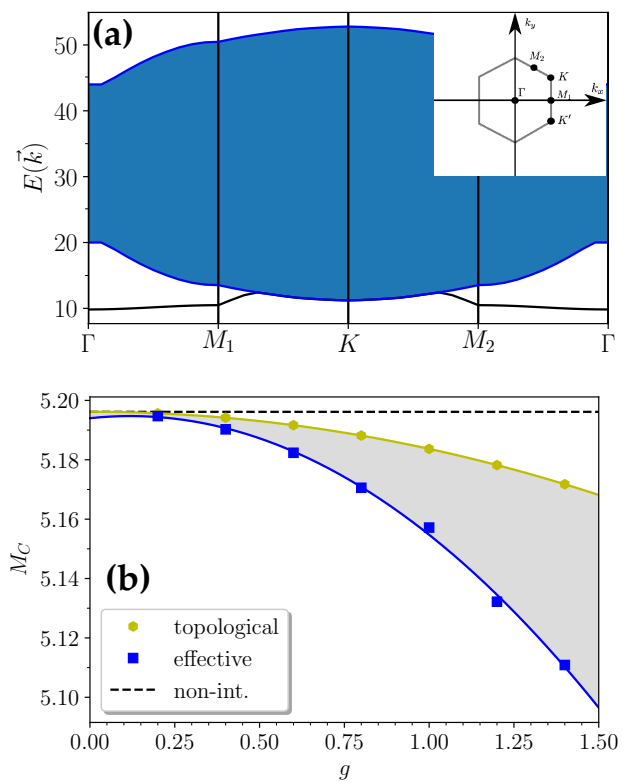


FIG. 2. (a) Two-boson continuum (colored) and renormalized single-boson bands for $E_0 = 16$, $M = 5.2$, and $g = 1.4$. (b) Critical values of M_C where the gap closes. Lines are quadratic fits.

The two-body approach in the full Hilbert space encounters the problem of a unique identification of the dressed single-boson states. We attempted to identify them by (a) maximizing the single-particle weight or by (b) maximizing the overlap of adjacent eigenvectors as function of wave vector in the BZ. But no reliable and numerical robust approach could be established. Hence, we cannot check independently whether the Chern number determined from the effective Hamiltonian possesses a physical

meaning in the full Hilbert space. In addition, we investigated the existence of localized edge modes for non-zero effective Chern number. Both the IPR and the LDOS indicate that the potential edge modes delocalize since they are not protected by an energy gap for overlapping bands, see Suppl. Mat. [56]. Hence, bands overlapping with continua appear to lose their particular topological properties, in line with the scenario on the single-particle level [36, 37] in the absence of protecting energy gaps.

Conclusions We have studied the topological properties of an interacting bosonic model on the honeycomb lattice allowing for the decay of a boson to two bosons and the inverse fusion. While the ground state (vacuum) is topologically trivial, the excited states are not. We investigated how Chern numbers C can be defined for these states and if edge states exist for non-vanishing C .

If the single-boson states are renormalized by the continuum without overlap in energy, Chern numbers can be computed either in the many-body Hilbert space with the full Hamiltonian or in the single-boson space with the bilinear Hamiltonian plus the self-consistent self-energy (effective Hamiltonian). It is the first key finding that these two approaches agree while taking the self-energy at zero energy does not agree. This agreement of the effective self-consistent calculation with the correct Berry phases is corroborated by an analytic derivation. Furthermore, our results indicate that the bulk-boundary correspondence holds in this case.

If both single-boson bands lie energetically *within* the two-boson continuum, one can extend the effective determination to the non-Hermitian case. The Chern number changes at gap closure which turns out to be an exceptional point. In spite of intensive search, we could not establish a robust definition of Berry phases in the full many-body Hilbert space. This sheds doubts on the significance of non-trivial Chern numbers in case of energetic overlaps. These doubts are enhanced by the absence of edge modes indicated by our numerical results with vanishing IPR and delocalized LDOS.

Our findings put the concept of non-trivial topology on a firm ground in presence of interactions inducing continua. If the eigenstates are only renormalized by the hybridization with continua, Chern numbers and the bulk-boundary correspondence apply as in the non-interacting case. If the single-particle states overlap with many-particle continua the concept of Chern numbers can be extended to non-Hermitian effective Hamiltonians. However, the Chern numbers are no longer protected by energy gaps and no localized edge modes seem to exist. This implies that an unambiguous definition of Berry phases in the full Hilbert space is no longer possible.

B.H. is grateful to the University of Manitoba and the Department of Physics and Astronomy for their hospitality and to the Studienstiftung des Deutschen Volkes for fi-

ancial support. J.S. acknowledges support by the Natural Sciences and Engineering Research Council (NSERC, Canada) and by the Deutsche Forschungsgemeinschaft (DFG) in Research Unit FOR 2316. G.S.U thanks the DFG for support in UH 90-14/1.

* bilal.hawashin@tu-dortmund.de

† sirker@physics.umanitoba.ca

‡ goetz.uhrig@tu-dortmund.de

- [1] K. v. Klitzing, G. Dorda, and M. Pepper, New Method for High-Accuracy Determination of the Fine-Structure Constant Based on Quantized Hall Resistance, *Phys. Rev. Lett.* **45**, 494 (1980).
- [2] D. J. Thouless, M. Kohmoto, M. P. Nightingale, and M. den Nijs, Quantized Hall Conductance in a Two-Dimensional Periodic Potential, *Phys. Rev. Lett.* **49**, 405 (1982).
- [3] M. Kohmoto, Topological Invariant and the Quantization of the Hall Conductance, *Ann. of Phys.* **160**, 343 (1985).
- [4] J. Weis and K. von Klitzing, Metrology and microscopic picture of the integer quantum Hall effect, *Phil. Trans. R. Soc. A* **369**, 3954 (2011).
- [5] M. Klein and R. Seiler, Power-Law Corrections to the Kubo Formula Vanish in Quantum Hall Systems, *Commun. Math. Phys.* **128**, 141 (1990).
- [6] G. S. Uhrig, Ohm's Law in the Quantum Hall Effect, *Z. Phys. B* **82**, 29 (1991).
- [7] D. C. Tsui, H. L. Stormer, and A. C. Gossard, Two-Dimensional Magnetotransport in the Extreme Quantum Limit, *Phys. Rev. Lett.* **48**, 1559 (1982).
- [8] The Nobel Prize in Physics 1985 (1985).
- [9] The Nobel Prize in Physics 1998 (1998).
- [10] The Nobel Prize in Physics 2016 (2016).
- [11] A. P. Schnyder, S. Ryu, A. Furusaki, and A. W. W. Ludwig, Classification of topological insulators and superconductors in three spatial dimensions, *Phys. Rev. B* **78**, 195125 (2008).
- [12] S. Ryu, A. P. Schnyder, A. Furusaki, and A. W. W. Ludwig, Topological insulators and superconductors: tenfold way and dimensional hierarchy, *New Journal of Physics* **12**, 065010 (2010).
- [13] C.-K. Chiu, J. C. Y. Teo, A. P. Schnyder, and S. Ryu, Classification of topological quantum matter with symmetries, *Rev. Mod. Phys.* **88**, 035005 (2016).
- [14] T. L. Hughes, E. Prodan, and B. A. Bernevig, Inversion-symmetric topological insulators, *Phys. Rev. B* **83**, 245132 (2011).
- [15] C. Fang, M. J. Gilbert, and B. A. Bernevig, Entanglement spectrum classification of C_n -invariant noninteracting topological insulators in two dimensions, *Phys. Rev. B* **87**, 035119 (2013).
- [16] A. Alexandradinata, X. Dai, and B. A. Bernevig, Wilson-loop characterization of inversion-symmetric topological insulators, *Phys. Rev. B* **89**, 155114 (2014).
- [17] S. Ryu and Y. Hatsugai, Entanglement entropy and the Berry phase in the solid state, *Phys. Rev. B* **73**, 245115 (2006).
- [18] L. Fidkowski, Entanglement spectrum of topological insulators and superconductors, *Phys. Rev. Lett.* **104**, 130502 (2010).

- [19] K. Monkman and J. Sirker, Operational entanglement of symmetry-protected topological edge states, *Phys. Rev. Res.* **2**, 043191 (2020).
- [20] K. Monkman and J. Sirker, Entanglement properties of one-dimensional chiral topological insulators (2022), arXiv:2207.10558.
- [21] K. Monkman and J. Sirker, Symmetry-resolved entanglement: General considerations, calculation from correlation functions, and bounds for symmetry-protected topological phases (2023), arXiv:2307.05820.
- [22] F. D. M. Haldane, Model for a Quantum Hall Effect without Landau Levels: Condensed-Matter Realization of the “Parity Anomaly”, *Phys. Rev. Lett.* **61**, 2015 (1988).
- [23] M. König, S. Wiedmann, C. Brüne, A. Roth, H. Buhmann, L. W. Molenkamp, X.-L. Qi, and S.-C. Zhang, Quantum spin Hall insulator state in HgTe quantum wells, *Science* **318**, 766 (2007).
- [24] Y. Ando, Topological insulator materials, *J. Phys. Soc. Jpn.* **82**, 102001 (2013).
- [25] G. Jotzu, M. Messer, R. Desbuquois, M. Lebrat, T. Uehlinger, D. Greif, and T. Esslinger, Experimental realization of the topological Haldane model with ultracold fermions, *Nature* **515**, 237 (2014).
- [26] Z. Yue, X. Wang, and M. Gu, *Advanced Topological Insulators*, edited by H. Luo (Scrivener Publishing LLC, 2019) p. 45.
- [27] D. Kong, J. C. Randel, H. Peng, J. J. Cha, S. Meister, K. Lai, Y. Chen, Z.-X. Shen, H. C. Manoharan, and Y. Cui, Topological insulator nanowires and nanoribbons, *Nano Lett.* **10**, 329 (2010).
- [28] D. Kong and Y. Cui, Opportunities in chemistry and materials science for topological insulators and their nanostructures, *Nat. Chem.* **3**, 845 (2011).
- [29] Y. Tokura, K. Yasuda, and A. Tsukazaki, Magnetic topological insulators, *Nat. Rev. Phys.* **1**, 126 (2019).
- [30] S. M. Frolov, M. J. Manfra, and J. D. Sau, Topological superconductivity in hybrid devices, *Nat. Phys.* **16**, 718 (2020).
- [31] M. Malki and G. S. Uhrig, Topological magnetic excitations, *EPL* **132**, 20003 (2020).
- [32] M. Malki and G. S. Uhrig, Tunable edge states and their robustness towards disorder, *Physical Review B* **95**, 235118 (2017).
- [33] X. S. Wang, H. W. Zhang, and X. R. Wang, Topological Magnonics: A Paradigm for Spin-Wave Manipulation and Device Design, *Phys. Rev. Applied* **9**, 024029 (2018).
- [34] M. Z. Hasan and C. L. Kane, Topological insulators, *Rev. Mod. Phys.* **82**, 3045 (2010).
- [35] A. B. Bernevig and T. L. Hughes, *Topological Insulators and Topological Superconductors* (Princeton University Press, Princeton, 2013).
- [36] M. Malki, L. Splinter, and G. S. Uhrig, Absence of localized edge modes in spite of a non-trivial Zak phase in BiCu₂PO₆, *Phys. Rev. Res.* **1**, 033197 (2019).
- [37] M. Malki and G. S. Uhrig, Delocalization of edge states in topological phases, *Europhys. Lett.* **127**, 27001 (2019).
- [38] H. Shen, B. Zhen, and L. Fu, Topological Band Theory for Non-Hermitian Hamiltonians, *Phys. Rev. Lett.* **120**, 146402 (2018).
- [39] E. J. Bergholtz, J. C. Budich, and F. K. Kunst, Exceptional topology of non-Hermitian systems, *Rev. Mod. Phys.* **93**, 015005 (2021).
- [40] W. Wang, X. Wang, and G. Ma, Non-Hermitian morphing of topological modes, *Nature* **608**, 50 (2022).
- [41] N. Okuma and M. Sato, Non-Hermitian Topological Phenomena: A Review, *Annu. Rev. Condens. Matter Phys.* **14**, 83 (2023).
- [42] K. Monkman and J. Sirker, Hidden zero modes and topology of multiband non-hermitian systems (2024), arXiv:2405.09728.
- [43] M. V. Berry, Quantal phase factors accompanying adiabatic changes, *Proc. Roy. Soc. Lond.* **A 392**, 45 (1984).
- [44] Q. Niu, D. J. Thouless, and Y.-S. Wu, Quantized Hall conductance as a topological invariant, *Physical Review B* **31**, 3372 (1985).
- [45] Z. Wang, X.-L. Qi, and S.-C. Zhang, Topological Order Parameters Interacting Topological Insulators, *Phys. Rev. Lett.* **105**, 256803 (2010).
- [46] V. Gurarie, Single-particle Green’s functions and interacting topological insulators, *Physical Review B* **83**, 085426 (2011).
- [47] X. Chen, Z.-C. Gu, Z.-X. Liu, and X.-G. Wen, Symmetry-Protected Topological Orders in Interacting Bosonic Systems, *Science* **338**, 1604 (2012).
- [48] A. L. Chernyshev and M. E. Zhitomirsky, Spin waves in a triangular lattice antiferromagnet: Decays, spectrum renormalization, and singularities, *Physical Review B* **79**, 144416 (2009).
- [49] A. L. Chernyshev and P. A. Maksimov, Damped topological magnons in the kagome-lattice ferromagnets, *Phys. Rev. Lett.* **117**, 187203 (2016).
- [50] M. E. Zhitomirsky and A. L. Chernyshev, Spontaneous magnon decays, *Rev. Mod. Phys.* **85**, 219 (2013).
- [51] M. E. Zhitomirsky, Decay of quasiparticles in quantum spin liquids, *Physical Review B* **73**, 100404(R) (2006).
- [52] T. Fischer, S. Duffe, and G. S. Uhrig, Microscopic model for Bose-Einstein condensation and quasiparticle decay, *Europhys. Lett.* **96**, 47001 (2011).
- [53] L. B. Müller and G. S. Uhrig, Interacting triplons in frustrated spin ladders: Binding and decay in BiCu₂PO₆, *Physical Review B* **107**, L081102 (2023).
- [54] R. Shindou, R. Matsumoto, S. Murakami, and J.-I. Ohe, Topological chiral magnonic edge mode in a magnonic crystal, *Physical Review B* **87**, 174427 (2013).
- [55] V. Peano, M. Houde, C. Brendel, F. Marquardt, and A. A. Clerk, Topological phase transitions and chiral inelastic transport induced by the squeezing of light, *Nat. Comm.* **7**, 10779 (2016).
- [56] For details, see Supplemental Material.
- [57] T. Fukui, Y. Hatsugai, and H. Suzuki, Chern Numbers in Discretized Brillouin Zone: Efficient Method of Computing (Spin) Hall Conductances, *J. Phys. Soc. Jpn.* **74**, 1674 (2005).
- [58] Z. Wang and S.-C. Zhang, Simplified Topological Invariants for Interacting Insulators, *Phys. Rev. X* **2**, 031008 (2012).
- [59] Z. Wang and B. Yan, Topological Hamiltonian as an exact tool for topological invariants, *J. Phys.: Condens. Matter* **25**, 155601 (2012).
- [60] B. Kramer and A. MacKinnon, Localization: theory and experiment, *Reports on Progress in Physics* **56**, 1469 (1993).
- [61] M. Calixto and E. Romera, Inverse participation ratio and localization in topological insulator phase transitions, *J. Stat. Mech.: Theor. Exp.* , P06029 (2015).
- [62] D. G. Pettifor and D. L. Weaire, *The Recursion Method and its Applications*, Springer Series in Solid State Sciences, Vol. 58 (Springer Verlag, Berlin, 1985).

- [63] V. S. Viswanath and G. Müller, *The Recursion Method: Application to Many-Body Dynamics*, Lecture Notes in Physics, Vol. m23 (Springer-Verlag, Berlin, 1994).
- [64] J. Stoer and R. Bulirsch, *Einführung in die Numerische Mathematik II*, Heidelberger Taschenbücher, Vol. 114 (Springer-Verlag, Berlin, Heidelberg, New York, 1978).
- [65] N. J. Higham and H. Kim, Numerical analysis of a quadratic matrix equation, *IMA J. Num. Analysis* **20**, 499 (2000).

Supplemental Material

SELF-ENERGY

Performing a Fourier transform and switching to the diagonal basis of the bilinear Hamiltonian H_0 , the Hamiltonian reads

$$H = \sum_{\vec{k}, \alpha} E_\alpha(\vec{k}) \tilde{b}_{\vec{k}, \alpha}^\dagger \tilde{b}_{\vec{k}, \alpha} + \sum_{\vec{k}, \vec{q}} \sum_{\alpha, \beta, \gamma} \left(\tilde{g}_{\alpha\beta\gamma}(\vec{k}, \vec{q}) \tilde{b}_{\vec{k}+\vec{q}, \alpha}^\dagger \tilde{b}_{-\vec{q}, \beta}^\dagger \tilde{b}_{\vec{k}, \gamma} + \text{h.c.} \right). \quad (6)$$

Here, $b_{\vec{k}, \alpha} = \sum_\beta U(\vec{k})_{\alpha, \beta} \tilde{b}_{\vec{k}, \beta}$ where the unitary matrix $U(\vec{k})$ is chosen such that the bilinear part is diagonal with energies $E_\alpha(\vec{k}) = d_0(\vec{k}) + (-1)^\alpha d(\vec{k})$ for $\alpha \in \{1, 2\}$, $d(\vec{k}) = \sqrt{d_x(\vec{k})^2 + d_y(\vec{k})^2 + d_z(\vec{k})^2}$ and

$$d_0(\vec{k}) = 2t_2 \cos(\phi) \left(\cos(\vec{k} \cdot \vec{a}_1) + \cos(\vec{k} \cdot \vec{a}_2) + \cos(\vec{k} \cdot \vec{a}_3) \right) + E_0, \quad (7a)$$

$$d_x(\vec{k}) = t_1 \left(1 + \cos(\vec{k} \cdot \vec{a}_1) + \cos(\vec{k} \cdot \vec{a}_2) \right), \quad (7b)$$

$$d_y(\vec{k}) = t_1 \left(\sin(\vec{k} \cdot \vec{a}_1) + \sin(\vec{k} \cdot \vec{a}_2) \right), \quad (7c)$$

$$d_z(\vec{k}) = M + 2t_2 \sin(\phi) \left(\sin(\vec{k} \cdot \vec{a}_1) - \sin(\vec{k} \cdot \vec{a}_2) - \sin(\vec{k} \cdot \vec{a}_3) \right), \quad (7d)$$

where we chose the primitive vectors $\vec{a}_1 = \frac{1}{2}(3, \sqrt{3})^T$ and $\vec{a}_2 = \frac{1}{2}(3, -\sqrt{3})^T$. The coupling constants in this basis are given by

$$\tilde{g}_{\alpha\beta\gamma}(\vec{k}, \vec{q}) = \frac{g}{\sqrt{N}} \left((U(\vec{k} + \vec{q})_{1, \alpha})^* (U(-\vec{q})_{1, \beta})^* U(\vec{k})_{1, \gamma} + (U(\vec{k} + \vec{q})_{2, \alpha})^* (U(-\vec{q})_{2, \beta})^* U(\vec{k})_{2, \gamma} \right). \quad (8)$$

At $T = 0$, the spectral representation of the retarded Green's function reads

$$G_{\alpha\beta}(\vec{k}, \omega) = \langle 0 | b_{\vec{k}, \alpha} \frac{1}{\omega + i0^+ - H + \epsilon_0} b_{\vec{k}, \beta}^\dagger | 0 \rangle, \quad (9)$$

where ϵ_0 is the energy of the ground state $|0\rangle$; it is zero in our case. In the diagonal basis of H_0 for fixed \vec{k} the full Hamiltonian H on $\mathcal{H}(1) \oplus \mathcal{H}(2)$ reads

$$H(\vec{k}) = \begin{pmatrix} D(\vec{k}) & V^\dagger(\vec{k}) \\ V(\vec{k}) & A(\vec{k}) \end{pmatrix}. \quad (10)$$

Then, the self-energy can be exactly determined to be

$$\Sigma(\vec{k}, \omega) = V(\vec{k})^\dagger \left(\omega - D(\vec{k}) \right)^{-1} V(\vec{k}). \quad (11)$$

In components,

$$\Sigma(\vec{k}, \omega)_{\gamma, \delta} = \sum_{\vec{q}} \sum_{\alpha, \beta} C(\vec{k}, \vec{q}) \frac{\tilde{g}_{\alpha\beta\gamma}(\vec{k}, \vec{q})^* \tilde{g}_{\alpha\beta\delta}(\vec{k}, \vec{q})}{\omega + i0^+ - E_{\alpha}(\vec{k} + \vec{q}) - E_{\beta}(-\vec{q})}, \quad (12a)$$

$$\text{with } C(\vec{k}, \vec{q}) = \begin{cases} 2 & \text{if } \vec{k} + 2\vec{q} \in \bar{\mathcal{B}}, \\ 1 & \text{else.} \end{cases}, \quad (12b)$$

where $\bar{\mathcal{B}}$ denotes the reciprocal lattice.

This result can also be understood in perturbation theory at zero temperature. The only contributing diagram is shown in Fig. 3. Higher-order diagrams do not contribute since they would involve three or more propagators between two times which vanish due to the restriction of the Hilbert space to at maximum two bosons. Also, no vertex corrections occur.

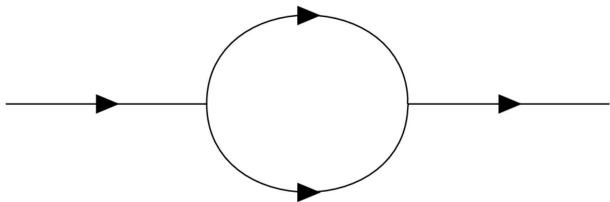


FIG. 3. The only diagrammatic contribution for the case $\mathcal{H} = \mathcal{H}(0) \oplus \mathcal{H}(1) \oplus \mathcal{H}(2)$, which is of second order in g . Neither higher-order diagrams nor vertex corrections are contributing for the considered restricted Hilbert space.

GENERALIZED LANCZOS TRIDIAGONALIZATION AND CONTINUED FRACTION REPRESENTATION

The numerical evaluation of the sum over the free momentum in Eq. (12b) depends on the discretization of the Brillouin zone. Generic results stay very spiky and do not allow for an interpretation based on a smooth imaginary part unless the δ -peaks are artificially broadened by a finite imaginary part of the frequency argument. To circumvent these issues, we generalize the continued fraction representation of scalar self-energies and propagators [62, 63] to matrices. As in the scalar case we find that an appropriate terminator leads to smooth multi-dimensional self-energies, essentially independent from the discretization, allowing for further evaluations as done in the main text.

We consider

$$\Sigma = V^\dagger (\omega - H)^{-1} V \quad (13)$$

where $V \in \mathbb{C}^{N \times d}$ and $H \in \mathbb{C}^{N \times N}$. Hence, the self-energy is a $d \times d$ matrix. The well-established scalar case

is recovered for $d = 1$. For the calculations in the main text we need $d = 2$, but the following derivation is valid for general d . The generalized Lanczos algorithm yields a block tridiagonal matrix with $d \times d$ blocks such that

$$H_T := U^\dagger H U = \begin{pmatrix} A_0 & B_1^\dagger & 0 & \dots \\ B_1 & A_1 & B_2^\dagger & \dots \\ 0 & B_2 & A_2 & \dots \\ \vdots & \vdots & \vdots & \ddots \end{pmatrix}, \quad (14)$$

with $A_i, B_i \in \mathbb{C}^{d \times d}$ and after L iterations, U is of the form

$$U = (V_0, V_1, \dots, V_L) \in \mathbb{C}^{N \times dL}. \quad (15)$$

The very starting point is defined by $V_0 = V$ if $V^\dagger V = \mathbb{1}_d$. Otherwise, we express $V = V_0 B_0$ by means of a standard QR-decomposition [64] where V_0 takes the role of Q and B_0 the role of R . Then, $V_0^\dagger V_0 = \mathbb{1}$ holds by construction.

We aim at a proof by induction over $n \in \mathbb{N}_0$. Hence, we assume that we have shown the following two relations up to and including $j, m \leq n$

$$V_j^\dagger V_m = \mathbb{1}_d \delta_{j,m} \quad \forall j, m \geq 0 \quad (16a)$$

$$V_j^\dagger H V_m = 0 \quad \forall |j - m| > 1. \quad (16b)$$

Base case For $n = 0$, V_0 has the desired property by construction and the structure of the Hamiltonian (14) implies

$$A_0 = V_0^\dagger H V_0. \quad (17)$$

Induction step Assuming that (16) holds up to n ,

$$A_j = V_j^\dagger H V_j \quad (18a)$$

$$B_j = V_j^\dagger H V_{j-1} \quad (18b)$$

holds by construction. To pass to $n + 1$ we consider

$$S_n = H V_n - V_n A_n - V_{n-1} B_n^\dagger = V_{n+1} B_{n+1}, \quad (19)$$

where the second equality refers to the QR-decomposition of S_n ; the diagonal elements of B_{n+1} are chosen to be positive. We exclude the possibility that one of these elements vanishes for the time being. Note that we set $V_{-1} := 0$ to maintain the general validity of this step.

We show (16a) in three steps. First, we multiply (19) from the left with V_n^\dagger yielding

$$V_n^\dagger V_{n+1} B_{n+1} = V_n^\dagger H V_n - V_n^\dagger V_n A_n - V_n^\dagger V_{n-1} B_n^\dagger \quad (20a)$$

$$= 0, \quad (20b)$$

where the first term on the right hand side of (20a) cancels with the second using (16a) and (18a) while the last one vanishes due to (16a). Thus, we know

$$V_n^\dagger V_{n+1} = 0 = V_{n+1}^\dagger V_n. \quad (21)$$

Second, we multiply (19) from the left with V_{n-1}^\dagger yielding

$$\begin{aligned} & V_{n-1}^\dagger V_{n+1} B_{n+1} \\ &= V_{n-1}^\dagger H V_n - V_{n-1}^\dagger V_n A_n - V_{n-1}^\dagger V_{n-1} B_n^\dagger \quad (22a) \\ &= 0, \quad (22b) \end{aligned}$$

where the first term on the right hand side of (22a) cancels with the last term using (16a) and (18b) while the second term vanishes due to (16a). Thus, we know

$$V_{n-1}^\dagger V_{n+1} = 0 = V_{n+1}^\dagger V_{n-1}. \quad (23)$$

Third, we multiply (19) from the left with V_m^\dagger with $0 \leq m < n-1$ which results in

$$\begin{aligned} & V_m^\dagger V_{n+1} B_{n+1} \\ &= V_m^\dagger H V_n - V_m^\dagger V_n A_n - V_m^\dagger V_{n-1} B_n^\dagger \quad (24a) \\ &= 0, \quad (24b) \end{aligned}$$

where the first term on the right hand side of (24a) vanishes due to (16b) and the second and third term vanish due to (16a). Thus, we know

$$V_m^\dagger V_{n+1} = 0 = V_{n+1}^\dagger V_m. \quad (25)$$

Hence, we know that (16a) holds also up to $n+1$.

What is left to complete the induction step is to prove $V_{n+1}^\dagger H V_m = 0$ for $0 \leq m < n$. To this end, we multiply (19) for $n=m$ from the left with V_{n+1}^\dagger yielding

$$0 = V_{n+1}^\dagger V_{m+1} B_{m+1} \quad (26a)$$

$$= V_{n+1}^\dagger H V_m - V_{n+1}^\dagger V_m A_m - V_{n+1}^\dagger V_{m-1} B_m^\dagger \quad (26b)$$

$$= V_{n+1}^\dagger H V_m. \quad (26c)$$

The first identity ensues from (16a) which we just have shown to hold. The second and third terms in (26b) vanish also due to (16a) so that the vanishing of the blocks beyond the minor diagonals in the Hamiltonian matrix is also extended to $n+1$. Recall that $V_m^\dagger H V_{n+1} = 0$ follows from hermiticity. This concludes the proof by induction.

Above, we assumed that the B_n always display the full rank of d . We point out that it can happen that for some $n = n_0$, one column of V_n vanishes. Then, the above algorithm reduces to a $(d-1)$ -dimensional Lanczos algorithm for $n > n_0$.

Multidimensional continued fraction expansion Given a basis in which H is block tridiagonal, we derive the continued fraction representation of the self-energy. We start for block matrices from the general identity

$$\begin{pmatrix} A & B \\ C & D \end{pmatrix}^{-1} = \begin{pmatrix} (A - B D^{-1} C)^{-1} & * \\ * & * \end{pmatrix}, \quad (27)$$

where we assume the existence of the inverse on the left hand side and of D^{-1} ; the blocks $*$ do not matter. Iterating this relation for the blocks of H_T we obtain

$$\Sigma = V^\dagger \frac{1}{\omega - H} V \quad (28a)$$

$$= B_0^\dagger P^\dagger \left(\frac{1}{\omega - H_T} \right) P B_0 \quad (28b)$$

$$= B_0^\dagger \left(\omega - A_0 - B_1^\dagger (\omega - A_1 - \dots)^{-1} B_1 \right)^{-1} B_0, \quad (28c)$$

where we have used $V = V_0 B_0$ and $P = (\mathbf{1}_d, 0)^\dagger \in \mathbb{C}^{N \times d}$. This relation can be expressed best as recursion

$$\Sigma_n = B_n^\dagger \frac{1}{\omega - A_n - \Sigma_{n+1}} B_n \quad (29)$$

with $\Sigma = \Sigma_0$. This provides the continued fraction expansion generalized to matrices.

Termination Finally, we discuss the issue of how to terminate the continued fraction expansion. Stopping at a finite depth of the fraction n_0 , i.e., setting $\Sigma_{n_0} = 0$ yields an imaginary part of the self-energy made up from a finite set of δ -distributions. For $d=1$ there are n_0 poles and generally we expect dn_0 poles. But this is still unsatisfactory because no smooth function is generated. In the scalar case of $d=1$ the square-root terminator, see Refs. [62, 63] as well as below in Eq. (36), allows one to terminate the continued fraction at finite depth while still yielding a smooth function. Here we briefly discuss whether an equivalent procedure is also possible in the multidimensional case. The answer is a yes, but less generally.

We assume that the following limits exist

$$\lim_{n \rightarrow \infty} A_n =: A_\infty, \quad \lim_{n \rightarrow \infty} B_n =: B_\infty \quad (30)$$

in the sense that each matrix element converges to a complex number. In order to derive a terminator, the following equation has to be solved

$$\Sigma_\infty = B_\infty^\dagger \frac{1}{\omega - A_\infty - \Sigma_\infty} B_\infty, \quad (31)$$

which is equivalent to

$$\Sigma_\infty B_\infty^{-1 \dagger} \Sigma_\infty - (\omega - A_\infty) B_\infty^{-1 \dagger} \Sigma_\infty + B_\infty = 0. \quad (32)$$

We multiply $B_\infty^{-1 \dagger}$ from the left and define

$$X := B_\infty^{-1 \dagger} \Sigma_\infty, \quad (33a)$$

$$O = -B_\infty^{-1 \dagger} (\omega - A_\infty) B_\infty^{-1 \dagger}, \quad (33b)$$

$$P := B_\infty^{-1 \dagger} B_\infty, \quad (33c)$$

to obtain the quadratic matrix equation

$$X^2 + OX + P = 0. \quad (34)$$

As discussed in Ref. [65], the solution of such an equation is not straightforward. For this reason, no general terminating procedure can be provided.

In our calculations, we observed, however, that often the block matrices A_n and B_n become more and more diagonal as n increases so that

$$(A_\infty)_{ij} = (B_\infty)_{ij} \approx 0 \quad \text{if } i \neq j. \quad (35)$$

Then, a simple solution suggests itself. The approximate diagonality of the Lanczos coefficients imply that $(\Sigma_\infty)_{ij} \approx 0$ so that Eq. 34 reduces to d independent equations for the diagonals, each solved by the standard square-root terminator

$$\Sigma_\infty = \begin{cases} \frac{\omega - a_\infty}{2} - \sqrt{\left(\frac{\omega - a_\infty}{2}\right)^2 - b_\infty^2}, & \omega > E_{\max}^{(2)}, \\ \frac{\omega - a_\infty}{2} - i\sqrt{b_\infty^2 - \left(\frac{\omega - a_\infty}{2}\right)^2}, & \omega \in [E_{\min}^{(2)}, E_{\max}^{(2)}], \\ \frac{\omega - a_\infty}{2} + \sqrt{\left(\frac{\omega - a_\infty}{2}\right)^2 - b_\infty^2}, & \omega < E_{\min}^{(2)}, \end{cases} \quad (36)$$

for real values of ω where $E_{\min/\max}^{(2)}$ corresponds to the minimum/maximum of the spectrum of H and a_∞ and b_∞ are the diagonal element of A_∞ and B_∞ , respectively. They are given by [62, 63]

$$a_\infty = (E_{\max}^{(2)} + E_{\min}^{(2)})/2 \quad b_\infty = (E_{\max}^{(2)} - E_{\min}^{(2)})/4. \quad (37)$$

For complex frequencies $z \in \mathbb{C}^+$, i.e., $\Im z > 0$, Σ_∞ is given by the retarded solution of the quadratic equation

$$\Sigma_\infty^2 - (z - a_\infty)\Sigma_\infty + b_\infty^2 = 0, \quad (38)$$

i.e., the one with negative imaginary part. This is the scalar version, i.e., for $d = 1$, of Eq. (32). In this work, we used this termination procedure as an approximation for the general matrix case yielding robust and smooth results.

EQUIVALENCE OF THE FULL EIGENVALUE PROBLEM AND THE SELF-CONSISTENT DIAGONALIZATION OF H_{eff}

We consider the Hilbert space consisting of the direct sum of the single-particle space $\mathcal{H}(1)$ and the remainder $\mathcal{H}_{\text{rest}}$. The Hamiltonian reads

$$H = H_1 + H_{\text{rest}} + H_V, \quad (39)$$

where H_1 only acts in $\mathcal{H}(1)$, H_{rest} only in $\mathcal{H}_{\text{rest}}$ while H_V links both according to $P_{\text{rest}}H_V P_1 = V$ where P_1 projects onto $\mathcal{H}(1)$ and P_{rest} projects onto $\mathcal{H}_{\text{rest}}$.

The full eigenvalue problem reads

$$H(v_1 + v_{\text{rest}}) = E(v_1 + v_{\text{rest}}) \quad (40)$$

where the vectors v_1 and v_{rest} live in $\mathcal{H}(1)$ and in $\mathcal{H}_{\text{rest}}$, respectively. Hence, (40) projected onto $\mathcal{H}(1)$ and onto $\mathcal{H}_{\text{rest}}$ yields

$$H_1 v_1 + V^\dagger v_{\text{rest}} = E v_1 \quad (41a)$$

$$H_{\text{rest}} v_{\text{rest}} + V v_1 = E v_{\text{rest}}. \quad (41b)$$

The second equation is equivalent to $(E - H_{\text{rest}})^{-1} V v_1 = v_{\text{rest}}$ which is well defined in Case I because we consider energies E in the range of the single-particle energies well below the lower continuum edge given by the lowest eigenvalue of H_{rest} . Inserting v_{rest} in the first equation (41a) yields

$$(H_1 + \Sigma(E))v_1 = E v_1, \quad (42)$$

where we use the self-energy $\Sigma(E) = V^\dagger(E - H_{\text{rest}})^{-1}V$. Clearly, the solution of (42) requires to find the self-consistency for E . Its solution is equivalent to solving the full eigenvalue problem (40).

EDGE STATES ON A HONEYCOMB RIBBON

To answer the question whether non-trivial Chern numbers imply edge states in the interacting case similar to the non-interacting case, we consider the model defined in Eq. (1) on the honeycomb ribbon with $N_x N_y$ sites as sketched in Fig. 4. One signature of localization is a finite inverse participation ratio I of eigenstate n defined by

$$I_n = \frac{\sum'_i |\psi_n^{(1)}(x_i, y_i)|^4}{\left(\sum'_i |\psi_n^{(1)}(x_i, y_i)|^2\right)^2}, \quad (43)$$

where $\psi_n^{(1)}(x_i, y_i)$ is the wave function of the n -th eigenstate projected onto $\mathcal{H}(1)$ in position space. Each site i has the spatial coordinates (x_i, y_i) . The sum \sum' runs over all y_i and the two x_i in the unit cell of the ribbon. From this definition, it is easy to see that a totally local state where only one site has the finite amplitude 1 yields $I_n = 1$ while a state completely delocalized over N states implies $I_n = 1/N$. In Fig. 5, we show the significantly different behavior of the IPR of a localized state and of a delocalized state.

In addition, we computed the local density of states (LDOS). The LDOS at zero temperature reads

$$A(x_i, y_i; \omega) = \sum_n |\langle n | b_i^\dagger | 0 \rangle|^2 \delta(\omega - E_n), \quad (44)$$

where $H|n\rangle = E_n|n\rangle$. Since we are interested in the localization at the edges $y = 0$ and $y = N_y - 1$, where N_y is the finite width of the ribbon in y direction, we additionally sum over the x_i coordinates, yielding

$$A(y_i; \omega) = \frac{1}{N} \sum_n \sum_{x_i} |\langle n | b_i^\dagger | 0 \rangle|^2 \delta(\omega - E_n), \quad (45)$$

which is the quantity of interest in the following.

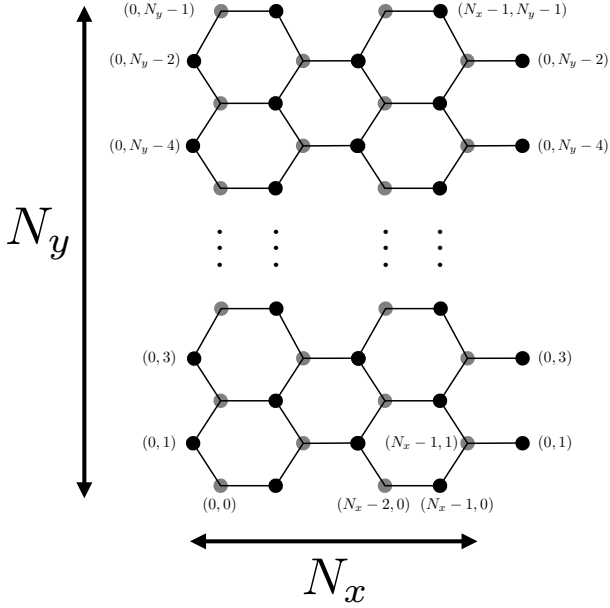


FIG. 4. Sketch of the considered lattice which is periodic in x direction (horizontal) with length N_x and has open boundary conditions and a finite length N_y in y direction (vertical). The total number of sites is $N_x N_y$ where N_x is even due to the basis of two sites and N_y is odd. The pair (i, j) denotes the position of the site with $0 \leq i < N_x$ and $0 \leq j < N_y$.

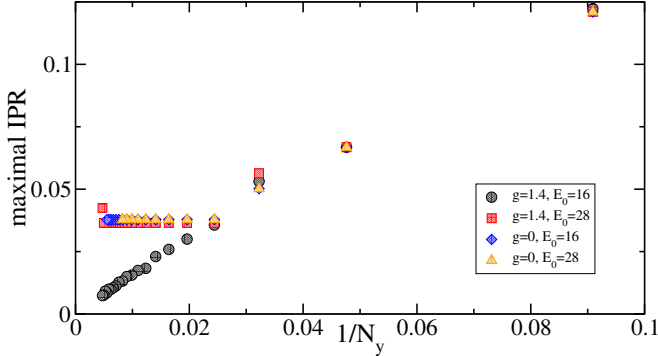


FIG. 5. IPR for a ribbon with $N_x = 2$ for vanishing and for finite interactions at parameters given in the legend. The states are localized without interaction and also in the interacting case for large $E_0 = 28$ avoiding energetic overlap. For small $E_0 = 16$ the overlap with the continuum leads to delocalization.

Non-interacting case For completeness and comparison, we first discuss the well-known non-interacting case of Eq. 1. We choose $N_x = 2$ and

$$t_1 = t_2 = 1, \phi = \frac{\pi}{2}, E_0 = 28. \quad (46)$$

As mentioned in the main text, the Chern number changes in this case from 1 to 0 at $M = 3\sqrt{3}$ upon increasing M . We show the spectrum of H as function of M in Fig. 6.

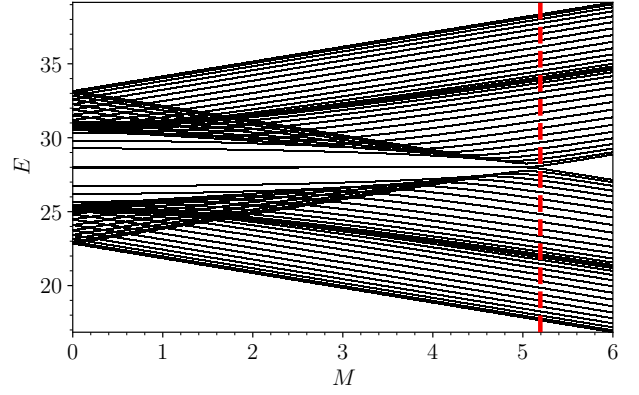


FIG. 6. Spectrum of the non-interacting model on a honeycomb ribbon with $N_x = 2, N_y = 33$. The vertical red line is the topological phase boundary at $M = 3\sqrt{3}$.

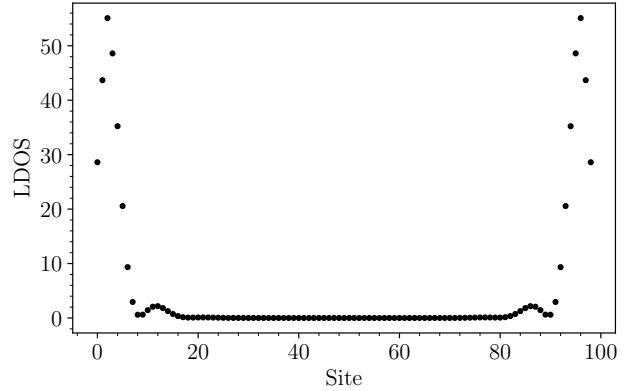


FIG. 7. LDOS of one of the two states with $E \approx E_0$ in the topological phase of the non-interacting model with $E \approx E_0$ and $M = 4.5$ for $N_x = 2$ and $N_y = 99$. Clearly, the state is localized at the edges of the system, illustrating the bulk-boundary correspondence.

The spectrum is symmetric around E_0 and we find two states with $E \approx E_0$, which are the well-known edge modes. Note that the two energies do not coincide perfectly because for any ribbon of finite width each state localized at one edge overlaps weakly with the state localized at the other edge. The true eigenstates are the symmetric and antisymmetric combination displaying a tiny, exponentially small energy splitting. The corresponding LDOS is shown in Fig. 7 for $M = 4.5$ implying $C = 1$. For $M > 3\sqrt{3}$ and thus $C = 0$, we find that the states lying energetically the closest to E_0 are not localized anymore and have their highest weight in the bulk (not shown).

Interacting case We turn on interactions and investigate the same interaction strength as considered in the main text, i.e., $g = 1.4$. We stress again, that $g \ll E_0$ and hence the interaction effects are still small compared to

the bare energies, i.e., the system is in the perturbative regime. In Fig. 8, we show the spectrum as a function of M for Case I of the main text, realized by choosing $E_0 = 28$.

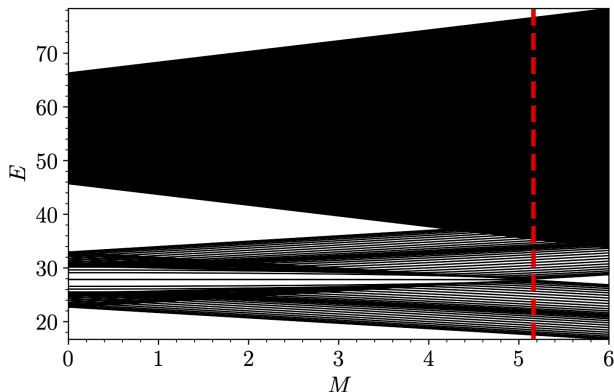


FIG. 8. Spectrum of the interacting system with $E = 28$ and $g = 1.4$, i.e., for Case I, with $N_x = 2$ and $N_y = 33$. The vertical red line is the topological phase boundary at $M = 5.162$, cf. Fig. 1.

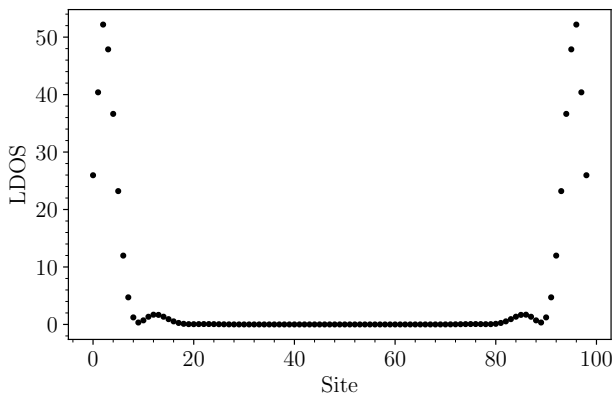


FIG. 9. LDOS of an edge state for the interacting case shown in Fig. 1 with $E \approx E_0 = 28$, i.e., Case I of the main text, and $N_x = 2, N_y = 99$ sites. The existence of edge states demonstrates that the bulk-boundary correspondence still applies in Case I.

We observe two important points:

- 1) Two states with energy $E \approx E_0$ still exist within the interacting spectrum.
- 2) The gap between the states above and below the two states with $E \approx E_0$ closes for a smaller value M_C than in the non-interacting case, which is consistent with Fig. 1.

Obvious candidates for edge states are again those with $E \approx E_0$. The LDOS of one of these states is displayed in Fig. 9 for $M = 4.5$ corresponding to Case I. We conclude

that in Case I where the two-particle continuum does not overlap with the single-particle bands of the bulk model, non-vanishing Chern numbers signal the existence of edge states as the bulk-boundary correspondence implies.

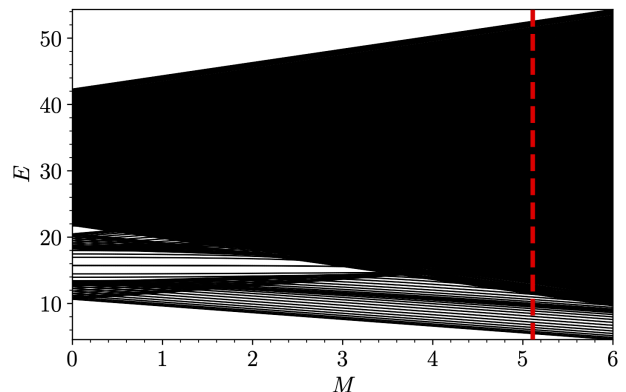


FIG. 10. Spectrum of the interacting system with $E_0 = 16$ and $g = 1.4$, i.e., for Case II, with $N_x = 2$ and $N_y = 33$. The vertical red line is the topological phase boundary at $M = 5.110$ determined from the self-consistent solution of the effective Hamiltonian.

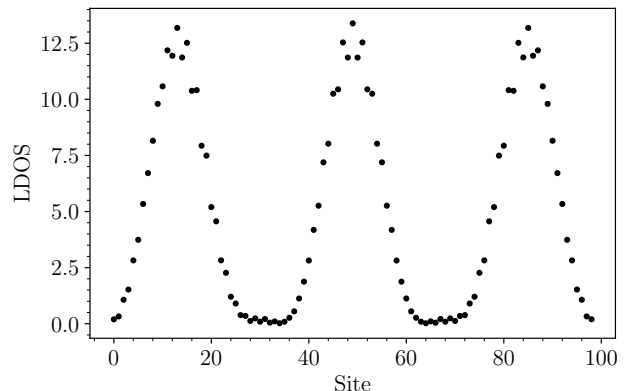


FIG. 11. LDOS of the state with the maximum IPR given that the spectral weight of the one-boson sector represents more than 50% of the total spectral weight for $N_x = 2$ and $N_y = 99$ with $M = 4.5$, i.e., for Case II.

Finally, we turn to Case II, where both bands overlap with the two-boson continuum. Note that we need $M > 3$ in order for the overlap to occur. The spectrum for this case is shown in Fig. 10. For $M > 3$, states with $E \approx E_0$ hybridize with the two-particle continuum and candidates for edge states cannot be determined straightforwardly. In this case, we consider the state with the maximum IPR among those states which have at least half their weight in the one-boson sector. In practice, we find that there is a clear distinction between predominantly single-particle states, where the single-particle weight is

larger than 98%, and the states which are predominantly of two-particle character. Some of the latter states have tiny one-particle contributions which appear to be localized. However, their LDOS is so minute that they do not influence the physics in any way. We study the scaling of the largest IPR among the preselected states with increasing width of the ribbon.

We choose $t_1 = t_2 = 1$, $\phi = \pi/2$, $E_0 = 16$, $g = 1.4$, and $M = 4.5$. This puts the system in the region where the analysis of the effective Hamiltonian indicates a non-zero Chern number while the single-particle bands are already hybridized with the continuum. The scaling of the largest IPR as a function of the length N_y is shown in Fig. 5 (black circles) indicating delocalization since this IPR clearly tends to zero for $N_y \rightarrow \infty$. This is strongly corroborated by Fig. 11 showing the LDOS of the state with maximal IPR. Obviously, this LDOS belongs to a delocalized standing wave as one might have expected due to the open boundary conditions. We conclude that the numerical data provide strong evidence that edge states delocalize when hybridizing with a continuum at the same energy.

TOPOLOGICAL PHASE TRANSITION AT AN EXCEPTIONAL POINT

In Case II, i.e., for overlap of the single bands with the continuum, the effective eigenvalue problem Eq. (3b) is no longer a hermitian one. Thus, the question arises which angle the two two-dimensional eigenvectors enclose. We studied this angle or the corresponding overlap, respectively, numerically across the closing of the gap at the K point in the BZ where the Chern number changes from 1 to 0 upon increasing M . The resulting data is depicted in Fig. 12.

The two eigenvalues merge at $M = 5.19$. Their eigenvectors are essentially perpendicular to each other, i.e., the non-hermiticity is hardly felt except for the vicinity of the topological phase transition. There the overlap quickly rises to (almost) unity which implies that the eigenvectors become parallel. This is the smoking gun characteristics of an exceptional point. Thus, our numerical data indicate that the topological transition in the case of overlapping bands and continua, i.e., in the non-Hermitian regime, occurs at exceptional points. We emphasize, however, that the frequency dependence of the effective Hamiltonian plays an important role and cannot be neglected.

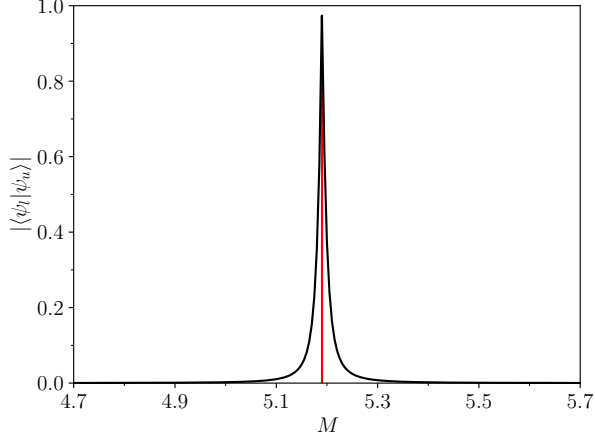


FIG. 12. Absolute value of the overlap given by the scalar product between the two eigenstates $|\psi_u\rangle$ and $|\psi_l\rangle$ corresponding to the eigenvalues $E_u \geq E_l$ at $g = 0.4$ and $E_0 = 16$ as function of the alternating potential M . The overlap is practically zero except for a narrow region around gap closure, marked by the vertical red line, which is accompanied by the change of the Chern number.